Magnetism in hybrid carbon nanostructures: Nanobuds

Xi Zhu[1] and Haibin Su[1,2,*]

[1]*Division of Materials Science, Nanyang Technological University, 50 Nanyang Avenue, Singapore 639798, Singapore*

[2]*Institute of High Performance Computing, 1 Fusionopolis Way, Connexis 138632, Singapore*

(Received 24 November 2008; revised manuscript received 11 March 2009; published 2 April 2009)

The robust magnetic state of recently synthesized hybrid carbon nanostructures, i.e., nanobuds, is predicted through comprehensive spin-polarized density-functional calculations. The effects of chirality, curvature, and topology on the magnetism of nanobuds are scrutinized by detailed electronic structure analysis. The substantial emergent amounts of unpaired spins originate in the presence of carbon radicals introduced by the geometry-induced electronic frustration. The location of radicals is mainly on the nanotube surface within the connecting region with fullerene, rather than surfaces with negative Gaussian curvature. The magnetic nanobuds hold great promise in the field of spintronics owing to their ready accessibility by experimental synthesis and fabrication.

DOI: 10.1103/PhysRevB.79.165401 PACS number(s): 75.75.+a, 73.22.−f, 75.70.−i

The worldwide intensive endeavors in spintronics[1,2] have renewed and stimulated tremendous interests in exploring carbon-based magnets, especially in the family of fullerene, carbon nanotube (CNT), and graphene.[3] The success of making such magnetic carbons is expected to turn the carbon nanoelectronics dramatically into a brand-new chapter with the full-fledged new degree of freedom, *spin*. Despite the suppression of one unpaired spin due to the strong covalent character in carbon systems, theoreticians have proposed various heuristic mechanisms[4–6] to explore the intriguing magnetic order in carbon materials. At the experimental side, Esquinazi *et al.*[7] unambiguously detected the ferromagnetic (FM) state in proton-irradiated graphite samples. While the fundamental microscopic mechanism of emergent magnetism is still under debate, notable factors, such as vacancies,[8] negative Gaussian curvature,[9] adatoms,[10] and terminal groups at edges,[11] are generally believed to be relevant ingredients to the magnetic state in carbon systems.

One approach for searching emergent properties is through assembled hybrid nanostructures.[12] One effective way of assembling fullerenes and CNTs into so-called peapod structures is by evaporating fullerene solids directly in the presence of CNTs without caps.[13] Upon heating or irradiation treatment, the peapod structure evolves into the Haeckelite tubular form[13,14] which is speculated to hold interesting magnetic properties.[15,16] Recently, Nasibulin *et al.*[17] applied CO disproportionation to synthesize fullerenes on iron-catalyst particles together with single-walled carbon nanotubes (SWNTs). Surprisingly, one type of emergent hybrid structure, termed a nanobud, is formed by welding fullerenes onto the outer surfaces of CNTs through covalent bonding.[17] Considering important versatile applications of both fullerenes and CNTs, this hybrid full carbon structure promises to have surely bright future. For instance, nanobud films have been shown to exhibit extremely high current density while being both optically transparent and flexible. This structure is quite attractive in view of its being immobile (in contrast to the mobile character of fullerene in peapod structures[18]) and its ready accessibility by experimental synthesis. So far, only the nonmagnetic (NM) electronic structure and transition states of various possible nanobud structures have been studied.[19] In this paper, we propose one family of nanobuds as excellent candidates for all-carbon magnets.

The geometries of nanobuds studied in this work are presented in Fig. 1. The six carbon atoms of CNT [yellow colored in Fig. 1(a)] establish covalent bonds to the fullerene. The sp^2 character of these carbon atoms is converted into sp^3. Thus, unpaired spins are expected to emerge in adjacent carbon atoms [blue colored in Fig. 1(a)], which are labeled by numbers from 1 to 7. The bonds associated with these atoms are indexed by alphabet letters: a, b, and c. To illustrate two covalent connections between CNTs and fullerene, we label two carbon atoms in the fullerene by u and v, and label three ones in the CNT by r, s, and t. The (u,v) atoms can form bonds with either (r,s) or (s,t) atoms, which then generate polygons in the neck area. Nonetheless, the topological nonequivalence is the most striking consequence of these two structures. When (u,v) atoms bond to (r,s) ones, a nine-membered ring (enneagon) is formed adjacent to a six-

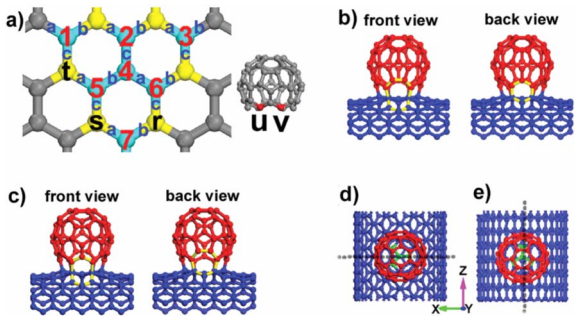

FIG. 1. (Color online) Geometric structures of one class of nanobuds. (a) The blue-colored carbon atoms of CNT host major unpaired spins. The yellow-colored carbon atoms of CNT connect the fullerene covalently. The topology is illustrated in detail in the text by atoms labeled as r, s, and t for CNT, and u and v for fullerene. Two topological structures of armchair CNT-based nanobuds: the yellow-colored bonds exhibit (b) nine- and six-membered rings in 9-6 case, and (c) eight- and seven-membered rings in 8-7 case. The top views of (d) armchair- and (e) zigzag-based nanobuds display the locations of the mirror planes, which can be visually observed by different orientations of three green-colored bonds as well.

TABLE I. Energetic data of a set of nanobuds with NM, FM, and AFM states, and the related formation reactions. The data inside parentheses are the total energies of nanobuds with double length along periodic direction. The relative energies of NM and AFM states are calculated by setting the energy of the ferromagnetic state of each nanobud to zero. The formation energy $E_{\text{formation}}$ is defined as $E(\text{nanobud})-E(C_{54})-E(\text{CNT})$, where $E(C_{54})$, $E(\text{CNT})$, and $E(\text{nanobud})$ are energies of C54, CNT, and the corresponding nanobud, respectively. A negative value of $E_{\text{formation}}$ means that the process of nanobud formation gives off heat.

Nanobud	E-NM (eV)	E-AFM (eV)	E-FM (eV)	$E_{\text{formation}}$ (eV)
8-7 (17,0)	0.57(−4688.71)	0.12(−4689.16)	0.00(−4689.28)	0.08
9-6 (17,0)	0.37(−4688.18)	−0.03(−4688.56)	0.00(−4688.54)	0.41
8-7 (10,10)	0.78(−4616.01)	0.20(−4616.60)	0.00(−4616.79)	−0.20
9-6 (10,10)	0.64(−4615.44)	0.16(−4615.91)	0.00(−4616.07)	0.15
8-7 (8,8)	0.54(−3872.20)	0.06(−3872.68)	0.00(−3872.74)	−0.88
9-6 (8,8)	0.47(−3871.56)	0.06(−3871.96)	0.00(−3872.02)	−0.87

membered ring (hexagon). We name it as 9-6 case as shown in Fig. 1(b). In comparison, the bonding between (u,v) and (s,t) atoms results in an eight-membered ring (octagon) paired with one adjacent seven-membered ring (heptagon), which is termed as 8-7 case as shown in Fig. 1(c). Furthermore, we literally choose armchair and zigzag CNTs in this work to represent the rich chirality character of CNTs. From geometric perspective, the top views of armchair- [in Fig. 1(d)] and zigzag-based nanobuds [in Fig. 1(e)] display the notable contrast in the mirror planes' locations. The mirror plane lies in the x-y plane (y-z plane) at the center of armchair (zigzag) CNT. This symmetry can be visually observed by different orientations of three green-colored bonds as well. Thus, we adopt the format of p-q (n,m), where p-q expresses the topology and (n,m) defines the CNT, to specify both chirality and topology of the nanobuds. Herein all calculations are performed within spin-polarized density-functional theory with the generalized gradient approximation of Perdew and Wang (PW91) functional[20] and plane-wave basis sets, which are nicely implemented in the Vienna *Ab Initio* Simulation Package (VASP).[21,22] The interaction between ions and electrons is treated by the frozen-core projector augmented wave (PAW) approach.[23] The energy cutoff is 400 eV, and the Monkhorst-Pack $1\times1\times5$ k-point grid is used to sample the Brillouin zone. The lengths of nanobuds along the periodic direction are 12.3 and 12.8 Å for armchair and zigzag types, respectively. The energetic data of nanobuds with NM, FM, and antiferromagnetic (AFM) states, and the related formation reactions are collected in Table I. It is important to point out that the five out of six nanobuds' ground state is ferromagnetic. Here, the fusion of C_{54} and CNT structures is assumed to form a nanobud for studying the formation energy $E_{\text{formation}}$, which is defined as $E(\text{nanobud})-E(C_{54})-E(\text{CNT})$, where $E(C_{54})$, $E(\text{CNT})$, and $E(\text{nanobud})$ are energies of C_{54}, CNT, and the corresponding nanobud, respectively. The negative values of $E_{\text{formation}}$ mean that the processes of forming 8-7 (10,10), 8-7 (8,8), and 9-6 (8,8) nanobuds give off heat. The heat required to form 8-7 (17,0), 9-6 (17,0), and 9-6 (10,10) nanobuds are 0.08, 0.41, and 0.15 eV, respectively. Since the amount of heat is very modest, which is less than 0.5 eV in the above three types of nanobuds, these hybrid nanostructures should be readily accessible experimentally.

Three geometrical factors are crucial in studying nanobuds' properties: the chirality of CNTs, the diameter of CNTs, and the topological connectivity. Let us first choose two nanobuds with the same CNT diameter (13.6 Å), 8-7 (17,0) and 8-7 (10,10), to investigate the chirality effect. Their spin-polarized band structures are sketched in Figs. 2(a) and 2(b). The bands between −1.0 and −0.5 eV have clear intrinsic CNT bands' character due to the symmetry.[24] We now focus on the flatbands associated with unpaired spins. The 8-7 (17,0) nanobud is metallic in both majority and minority sectors as shown in Fig. 2(a). The highest up-spin band runs gradually from 20 meV above E_F at Γ point to 86 meV below E_F at X point. The large portion of the lowest down-spin band is located a few meV below E_F. Only small part of this band lies within 10 meV above E_F at X point. For the 8-7 (10,10), a total of six relatively flat up-spin bands are almost totally below the Fermi level, while the down-spin bands are all above E_F as shown in Fig. 2(b). Note that there is one flatband around 0.4 eV above E_F in both majority and minority sectors for both nanobuds, which is formed by fullerene. Considering that s and $P_{z,x}$ orbitals

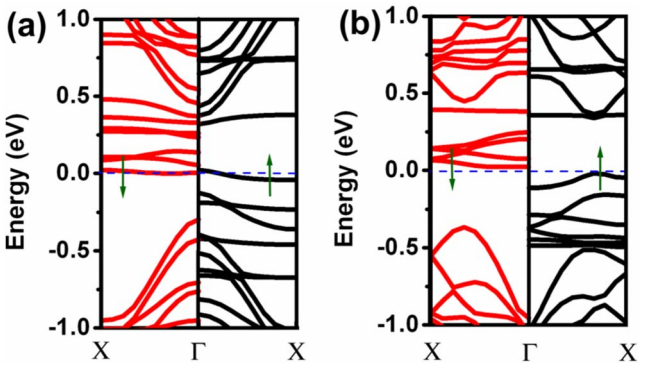

FIG. 2. (Color online) Electronic spin-polarized band structures of (a) 8-7 (17,0) and (b) 8-7 (10,10) nanobuds. The majority- (up-) spin bands are plotted at right parts with black color, while the minority- (down-) spin bands are plotted at left parts with red color. The Fermi energy is set to zero.

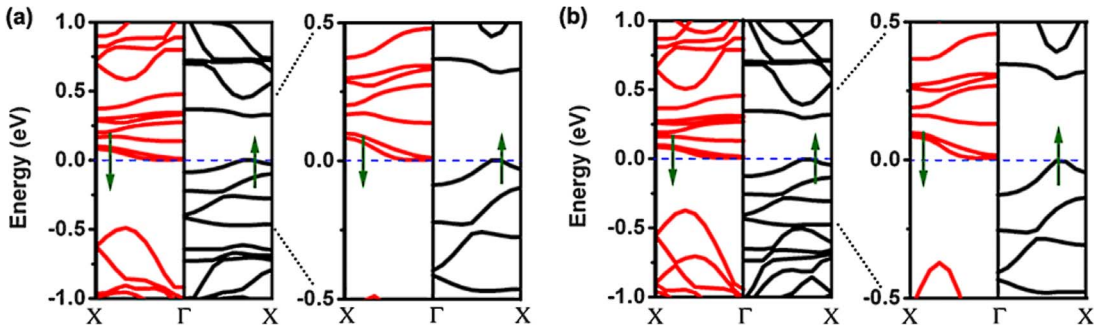

FIG. 3. (Color online) Electronic spin-polarized band structures of (a) 9-6 (8,8) and (b) 9-6 (10,10) nanobuds. The majority- (up-) spin bands are plotted at right parts with black color, while the minority- (down-) spin bands are plotted at left parts with red color. The Fermi energy is set to zero. The band structures at fine scale of both nanobuds are also presented to illustrate details near the Fermi surface.

form the sp^2 bonding network of CNTs, the unpaired electrons are expected to have unambiguous P_y character as unraveled by the projected density of states analysis. The band structures evidently exhibit that 8-7 (10,10) nanobud has approximate net magnetic moment of $6\mu_B$, while 8-7 (17,0) holds $4\mu_B$. Indeed, the more sophisticated integration in the first Brillouin zone yields $6.0\mu_B$ for the former and $4.25\mu_B$ for the latter.

Next we discuss the curvature effect. Although schwarzons (with negative Gaussian curvature[25,26]) clearly exist in nanobuds, here the curvature effect mainly refers to CNT since it is well known that the electronic structure can be altered in small CNTs due to the large hybridization effect.[27] The 9-6 (8,8) and 9-6 (10,10) nanobuds' band structures are plotted in Figs. 3(a) and 3(b). The diameter of (8,8) CNT is 10.9 Å, which is 2.6 Å smaller than that of (10,10). Consequently, the angle between adjacent P_y orbitals decreases from 24.2° in (8,8) to 13.9° in (10,10), which yields observable change in the spin-dependent exchange coupling. The effective strength of this type of exchange coupling could be indicated by the relative shift between majority and minority bands. The enhancement of coupling strength formally shifts down the highest up-spin band from (8,8) nanobud to (10,10) one by 12 meV in average as shown in the band structures at fine scale in Fig. 3. The magnetic moment of the 9-6 (10,10) nanobud turns out to be $5.95\mu_B$, which is $0.23\mu_B$ larger than that of the 9-6 (8,8) nanobud.

Third, the topological factor, referring to how the fullerene welds with CNTs as illustrated in Figs. 1(b) and 1(c), can play an important role in nanobuds' magnetism. Both topological connections, i.e., 9-6 and 8-7, preserve the σ_v symmetry in the x-y plane (y-z plane) at the center of structure of an armchair (zigzag) nanotube. The topological effect can be demonstrated by the nature of ground state and detailed band structure. Note that the ground state of 8-7 (17,0) nanobud is the ferromagnetic state. The ground state of the 9-6 (17,0) one is, however, an antiferromagnetic one with 30 meV lower in energy than the corresponding ferromagnetic state of 9-6 (17,0) nanobud as in Table I. The perturbation of band structures due to the topological factor is analyzed with (10,10) nanobuds. Although the net magnetic moments are almost unchanged between 8-7 and 9-6 (10,10), the three lowest up-spin bands show distinctive distributions in Figs. 2(b) and 3(b). These three bands are quite compactly distributed near −0.5 eV in 8-7 (10,10) as shown in Fig. 2(b). Interestingly, the two lowest are shifted down further by about 200 meV in 9-6 (10,10) as presented in Fig. 3(b). Due to the larger average bond deformation in the 9-6 topology than that in 8-7 topology, we believe that the topology-dependent bond strain accounts for the delicate change in the sign and strength of exchange coupling in the nanobuds.

The spin densities are plotted in Figs. 4(a)–4(d). Note that the yellow-colored carbon atoms presented in Fig. 1(a) are sp^3 carbons attributed to the covalent bonding between the fullerene and CNT. Their adjacent carbon atoms have to respond to this imposed constraint, which is nicely reflected by the change in associated bond lengths. For instance, the bond lengths of 1b and 1c elongate from 1.42 Å (as in perfect CNTs) to 1.49 Å in 8-7 (10, 10) nanobud, which causes the carbon atom 1 (C-1) to carry certain amount of unpaired spin

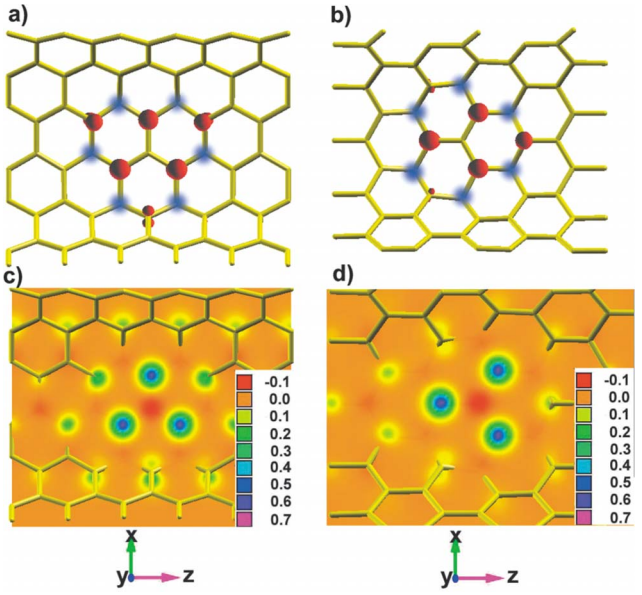

FIG. 4. (Color online) Isosurfaces of spin density (0.2 $e/\text{Å}^3$) denoted by red lobes and spin- density contour ($e/\text{Å}^2$) of [(a) and (c)] 8-7 (10,10) and [(b) and (d)] 8-7 (17,0) nanobuds. The blue-colored carbon atoms of CNTs, shown in (a) and (b), connect covalently to the fullerenes, which is not shown here for clarity.

component. Similar analysis holds for C-2 to C-7. For the half-filled case, the spin alignment usually observes the even-odd type topological rule.[28,29] However, the boundary imposed by the six sp^3 carbons generates the geometry-induced electronic frustration that leads to carbon radicals in the high-spin configuration. The location of radicals (i.e., C-1 to C-7) on CNTs with positive curvature in nanobuds is remarkably different from the carbon tetrapods, where radicals are in the core surface with negative curvature.[9] Equally important, the schwarzons are expected to provide effective shielding for these carbon radicals so as to enhance their stability. These unpaired spins, as shown in Fig. 4, are the main source for the magnetic state in nanobuds. The direct counting yields a magnetic moment of about $6\mu_B$ for 8-7 (10,10). For the 8-7 (17,0) structure, once we rotate the fullerene 90° along y axis to establish geometric connection with 8-7 (10,10), we find that the two patterns share the main features. However, the quantitative spin population is different. The 8-7 (17,0) clearly has less spin density. Thus the total moment is reduced to approximate $4\mu_B$.

In summary, we propose the magnetic state of one family of all-carbon nanobuds. Our spin-polarized density-functional calculations reveal the existence of substantial amount of unpaired spins originating in the presence of carbon radicals introduced by the geometry-induced electronic frustration. The location of radicals is mainly on the nanotube surface within the connecting region with fullerene, rather than surfaces with negative Gaussian curvature. Detailed electronic analysis clearly demonstrates the influences of chirality, curvature, and topology on the net magnetic moment and exchange coupling in nanobuds. The optimization in the experiment process is needed to achieve the controllable synthesis of nanobuds with desired geometries. More importantly, the delicate magnetic coupling among the assembled nanobuds' network deserves further extensive investigations. Considering the extremely intrinsic weak spin-orbital coupling, the uncontaminated magnetic nanobuds hold good promise in the field of spintronics.

H.S. thanks Markus Reiher at ETH Zurich and Andrew Horsfield at Imperial College London for interesting discussions. Work at NTU was supported in part by an A*STAR PSF grant (Grant No. 0621010030) and MOE AcRF-Tier-1 grant (Grant No. M52070060).

*hbsu@ntu.edu.sg

[1] S. A. Wolf, D. D. Awschalom, R. A. Buhrman, J. M. Daughton, S. von Molnar, M. L. Roukes, A. Y. Chtchelkanova, and D. M. Treger, Science **294**, 1488 (2001).

[2] I. Zutic, J. Fabian, and S. Das Sarma, Rev. Mod. Phys. **76**, 323 (2004).

[3] *Carbon-Based Magnetism*, edited by T. Makarova and F. Palacio (Elsevier, Amsterdam, 2006).

[4] A. N. Andriotis, M. Menon, R. M. Sheetz, and L. Chernozatonskii, Phys. Rev. Lett. **90**, 026801 (2003).

[5] Y. W. Son, M. L. Cohen, and S. G. Louie, Nature (London) **444**, 347 (2006).

[6] F. Cervantes-Sodi, G. Csányi, S. Piscanec, and A. C. Ferrari, Phys. Rev. B **77**, 165427 (2008); O. Hod, V. Barone, and G. E. Scuseria, *ibid.* **77**, 035411 (2008).

[7] P. Esquinazi, D. Spemann, R. Hohne, A. Setzer, K. H. Han, and T. Butz, Phys. Rev. Lett. **91**, 227201 (2003).

[8] P. O. Lehtinen, A. S. Foster, Y. Ma, A. V. Krasheninnikov, and R. M. Nieminen, Phys. Rev. Lett. **93**, 187202 (2004); Y. Zhang, S. Talapatra, S. Kar, R. Vajtai, S. Nayak, and P. M. Ajayan, *ibid.* **99**, 107201 (2007).

[9] N. Park, M. Yoon, S. Berber, J. Ihm, E. Osawa, and D. Tomanek, Phys. Rev. Lett. **91**, 237204 (2003).

[10] P. O. Lehtinen, A. S. Foster, A. Ayuela, A. Krasheninnikov, K. Nordlund, and R. M. Nieminen, Phys. Rev. Lett. **91**, 017202 (2003).

[11] E. J. Kan, Z. Y. Li, J. L. Yang, and J. G. Hou, J. Am. Chem. Soc. **130**, 4224 (2008).

[12] H. Zheng, J. L. Wang, S. Lofland, Z. Ma, L. Mohaddes-Ardabili, T. Zhao, L. Salamanca-Riba, S. R. Shinde, S. B. Ogale, F. Bai, D. Viehland, Y. Jia, D. G. Schlom, M. Wuttig, A. Roytburd, and R. Ramesh, Science **303**, 661 (2004); C. K. Yang, J. Zhao, and J. P. Lu, Phys. Rev. Lett. **90**, 257203 (2003); Y. Yagi, T. M. Briere, M. H. F. Sluiter, V. Kumar, A. A. Farajian, and Y. Kawazoe, Phys. Rev. B **69**, 075414 (2004).

[13] B. W. Smith, M. Monthioux, and D. E. Luzzi, Nature (London) **396**, 323 (1998); B. W. Smith and D. E. Luzzi, Chem. Phys. Lett. **321**, 169 (2000); E. Hernandez, V. Meunier, B. W. Smith, R. Rurali, H. Terrones, M. B. Nardelli, M. Terrones, D. E. Luzzi, and J. C. Charlier, Nano Lett. **3**, 1037 (2003).

[14] H. B. Su, R. J. Nielsen, A. C. T. van Duin, and W. A. Goddard III, Phys. Rev. B **75**, 134107 (2007).

[15] L. Liu, G. Y. Guo, C. S. Jayanthi, and S. Y. Wu, Phys. Rev. Lett. **88**, 217206 (2002).

[16] J. A. Rodríguez-Manzo, F. López-Urías, M. Terrones, and H. Terrones, Nano Lett. **4**, 2179 (2004).

[17] A. G. Nasibulin, P. V. Pikhitsa, H. Jiang, D. P. Brown, A. V. Krasheninnikov, A. S. Anisimov, P. Queipo, A. Moisala, D. Gonzalez, G. Lientschnig, A. Hassanien, S. D. Shandakov, G. Lolli, D. E. Resasco, M. Choi, D. Tománek, and E. I. Kauppinen, Nat. Nanotechnol. **2**, 156 (2007); A. G. Nasibulin, A. S. Anisimov, P. V. Pikhitsa, H. Jiang, D. P. Brown, M. Choi, and E. I. Kauppinen, Chem. Phys. Lett. **446**, 109 (2007).

[18] H. B. Su and W. A. Goddard III, Nanotechnology **17**, 5691 (2006).

[19] T. Meng, C. Y. Wang, and S. Y. Wang, Phys. Rev. B **77**, 033415 (2008); X. J. Wu and X. C. Zeng, ACS Nano **2**, 1459 (2008).

[20] J. P. Perdew, K. Burke, and Y. Wang, Phys. Rev. B **54**, 16533 (1996).

[21] G. Kresse and J. Furthmuller, Phys. Rev. B **54**, 11169 (1996); Comput. Mater. Sci. **6**, 15 (1996).

[22] G. Kresse and J. Hafner, Phys. Rev. B **48**, 13115 (1993); **49**, 14251 (1994).

[23] P. E. Blochl, Phys. Rev. B **50**, 17953 (1994); G. Kresse and D. Joubert, *ibid.* **59**, 1758 (1999).

[24] R. Saito, G. Dresselhaus, and M. S. Dresselhaus, *Physical Prop-*

erties of Carbon Nanotubes (Imperial College, London, 1998).
[25] T. Lenosky, X. Gonze, M. Teter, and V. Elser, Nature (London) **355**, 333 (1992).
[26] G. E. Scuseria, Chem. Phys. Lett. **195**, 534 (1992).
[27] X. Blase, L. X. Benedict, E. L. Shirley, and S. G. Louie, Phys. Rev. Lett. **72**, 1878 (1994).
[28] N. Mataga, Theor. Chim. Acta **10**, 372 (1968).
[29] E. H. Lieb, Phys. Rev. Lett. **62**, 1201 (1989).